Author Manuscript

**Title:** One-step Rapid and Scalable Flame Synthesis of Efficient WO3 Photoanodes for Water Splitting

**Authors:** Antonio Tricoli, Dipl. Ing. ETH, PhD ETH Zurich; Hongjun Chen; Renheng Bo; Thanh Tran; Guanyu Liu



**To be cited as:** ChemPlusChem 10.1002/cplu.201800061

**Link to VoR:** https://doi.org/10.1002/cplu.201800061

# One-step Rapid and Scalable Flame Synthesis of Efficient $WO_3$ Photoanodes for Water Splitting

*Hongjun Chen[a]*, Renheng Bo[a], Thanh Tran-Phu[a], Guanyu Liu[ab] and Antonio Tricoli[a]**

[a]Nanotechnology Research Laboratory, Research School of Engineering, Australian National University, Canberra 2601, Australia.
[b]CSIRO, Black Mountain, Canberra 2601, Australia

**ABSTRACT:** Photoelectrochemical water splitting is a promising approach for the carbon-free production of hydrogen from sun light. Here, robust and efficient $WO_3$ photoanodes for water oxidation were synthesized by scalable one-step flame synthesis of nanoparticle aerosols and direct gas-phase deposition. Nanostructured $WO_3$ films with tunable thickness, bandgap and controllable porosities were fabricated controlling the aerosol deposition time, concentration and temperature. Optimal $WO_3$ films demonstrate superior water oxidation performance reaching a current density of 0.91 mA at 1.24 V vs. reversible hydrogen electrode (RHE) and an IPCE of ~ 61% at 360 nm in 0.1 M $H_2SO_4$ solution. Notably, it is found that the excellent performance of these $WO_3$ nanostructures arises from the high in-situ restructuring temperature (~1000 °C), which increases oxygen vacancies and decreases charge recombination at the $WO_3$/electrolyte interface. These findings provide a scalable approach for the fabrication of efficient $WO_3$ and other metal oxides-based photoelectrodes for light-driven water splitting.

**KEYWORDS:** *one-step, scalable, robust, photoelectrochemical, water splitting, flame synthesis, $WO_3$,*



**Corresponding authors: antonio.tricoli@anu.edu.au; hongjun.chen@anu.edu.au;*

Solar-driven photoelectrochemical (PEC) water splitting has been extensively studied as a means for production of solar hydrogen as a renewable and sustainable energy carrier.[1] Low-cost earth-abundant semiconductors such as $TiO_2$, ZnO, hematite and $WO_3$[2] are increasingly investigated as photoelectrodes Nanostructured $WO_3$ is particularly attractive due to its suitable bandgap, high electron mobility, and low cost.[3] The $WO_3$ bandgap of 2.6-2.8 eV can utilize ~12% solar light with a theoretical photocurrent density of ~ 4 mA $cm^{-2}$.[4] In order to develop highly efficient $WO_3$ photoanodes, several techniques have been employed to fabricate tailored nanostructures such as sputtering, chemical vapour deposition, electrodeposition, anodic oxidization, sol-gel and hydrothermal methods.[2c, 3b, 5] In addition to nanoparticles, various other $WO_3$ nanostructures like nanowires, nanoplates, nanosheets, and nanoflakes have also been developed through hydrothermal methods.[2c, 5e-i] Often, a post-calcination treatment or multiple steps with limited scalability are required to further increase the crystallinity of the $WO_3$ nanostructures for enhancement of their PEC performance. The development of a one-step scalable method for the fabrication of efficient $WO_3$ photoanode is beneficial to facilitate its future implementation for PEC water splitting.

Flame synthesis is an established technology for the commercial production of nanoparticles like carbon black, fumed silica and other nanoparticle commodities.[6] Recently, flame synthesis of nanoparticle aerosols and direct deposition has been applied to the fabrication of ultraporous networks of metal oxide semiconductors for optoelectronic devices.[7] Such films consist of ultrafine nanoparticles and can be rapidly synthesized and directly deposited with more than 90%.[8] However, a major limitation of such films is their poor mechanical stability due to their high porosity. Further optimization of the structural properties of these films is required for the fabrication of robust photoelectrodes for their application water splitting.

Here, a one-step rapid flame synthesis and deposition method for the fabrication of $WO_3$ photoelectrodes with tunable thickness, bandgap, and controllable porosities is introduced. It was observed that a short nanoparticle aerosol deposition time of 10 s is sufficient to fabricate robust $WO_3$ films on FTO substrate without the need of any post-calcination treatment. Optimal $WO_3$ nanostructured films show superior PEC performance reaching a current density of 0.91 $mAcm^{-2}$ at 1.24 V vs RHE with

a maximum IPCE of ca. 61% at 360 nm. This performance has been attributed to their higher donor densities and efficient charge transfer at the $WO_3$/electrolyte interface.

## RESULTS AND DISCUSSION

The morphologies of $WO_3$ deposited at different height above the burner (HAB) are shown in Figure 1. As shown in Figure 1b, e and h, $WO_3$ nanocrystals are agglomerated into cauliflower structures and uniformly distributed on the substrates, which is quite similar to previously reported for flame-made ZnO films.[9] With decreasing the HAB from 10 to 6 cm, the film becomes much denser and the intra-agglomerate pores decrease from ~1-2 µm at HAB of 10 cm to less than 100 nm at HAB of 6 cm. Meanwhile, at higher magnification (Figure1a, d and g), the $WO_3$ nanocrystals within cauliflower structures increase in size. Therefore, the interspace among $WO_3$ nanocrystals within cauliflower structure is much denser at HAB of 6 cm than those formed at HAB of 8 and 10 cm. The cross-section SEM images of the films are presented in Figure 1c, f and i. The $WO_3$ films deposited at HAB of 8 and 10 cm demonstrate tree-like micro-sized structure that extended throughout the film cross-section terminating in cauliflower-like tips. The thickness of $WO_3$ films are ca. 1.5, 1.5, 2.5 µm for the HAB of 6, 8 and 10 cm, respectively. The $WO_3$ film deposited at HAB of 6 cm appears more robust than those deposited at HAB of 8 and 10 cm, and its morphology is different from those previously obtained by deposition of flame-made nanoparticle aerosols[8a] at HAB of 20 cm.

The composition and crystallinity of these $WO_3$ films were investigated by energy-dispersive spectrum (EDS) and X-ray diffraction (XRD). As shown in Figure 2a, the elements of W and O can be clearly seen in the EDS spectra, while other elements like Sn and trace amount of C comes from FTO substrate and probably atmospheric $CO_2$ adsorption, respectively. Figure 2b shows XRD patterns which reveal that the crystal structures of $WO_3$ films with different HAB are monoclinic $WO_3$ (JCPDS No. 72-0677) with typical peaks located at 23.2°, 23.8° and 24.5° corresponding to the (002), (020) and (200) facets.[2c, 10] In addition to XRD peaks of FTO substrate, no other peaks can be observed, indicating that all films are pure monoclinic $WO_3$. From XRD analysis, the average crystal sizes of $WO_3$ are computed to ca. 19.6, 34.7 and 44.3 nm for the HAB of 10, 8 and 6 cm, respectively. Notably, the relative intensity of the (020) diffraction peak in the $WO_3$ film at HAB of 6 cm is much higher than that of the other peaks, suggests

that $WO_3$ nanocrystals are partially aligned along the [020] direction,[2c, 10] which is different from the other two $WO_3$ films deposited at HAB of 8 and 10 cm. The preferential orientation of $WO_3$ nanocrystals in [020] direction is attributed to the increasing deposition temperature at lower HAB, due to the heating from the hot flame aerosol. This is in line with reports indicating that high calcination temperature promotes $WO_3$ growth in the [020] direction.[11]

The optical properties of flame-made $WO_3$ films were investigated by UV-vis absorption. Figure 2c shows the UV-vis spectra of $WO_3$ films obtained at different HAB and a wide absorbance between ca. 450 to 200 nm can be clearly seen in these spectra. Meanwhile, the onset absorbance is gradually red-shifted with HAB decreased from 10 to 8 then to 6 cm, suggesting the bandgap gradually reduced with the decrease of HAB.[2c, 2e] In order to deduce the bandgap of these $WO_3$ films, Tauc plot (shown in Figure 2d) was applied. The bandgap of these three different $WO_3$ films are 2.68, 2.69 and 2.77 eV for $WO_3$ at HAB of 6, 8 and 10 cm, respectively. From the comparison, it can be seen that the bandgap of $WO_3$ at HAB of 6 cm is comparable with that of $WO_3$ at HAB of 8 cm after post-calcination treatment, but still narrower than that of $WO_3$ at HAB of 10 cm. The variable bandgap of $WO_3$ at different HAB is connected with their flame deposition condition and further post-calcination treatment applied to the HAB 8 and 10 cm only (Figure S1).[2e] From the above characterizations, therefore, it can be concluded that different deposition HAB, and thus temperature and oxygen partial pressure, influences the morphology, the crystal structure, and the optical properties of the $WO_3$ films.

In order to optimize the films' optical density, $WO_3$ films with different flame aerosol deposition time were deposited on FTO at HAB of 6 cm. As shown in Figure 3a, the photocurrent density during water oxidation increased when the flame deposition time increased from 5 to 10 s, and then gradually decreased if extending the deposition time to 20 and 30s, which indicates that 10 s is the optimal deposition time at HAB of 6 cm reaching a current density of 0.91 mA $cm^{-2}$ at 1.24 V vs. RHE in 0.1 M $H_2SO_4$. The change of current density for $WO_3$ films with different deposition time might be closely connected with the light penetration depth in $WO_3$ film (the transmittance spectra and optical density is shown in Figure S2) and the resistance change of the FTO substrate during flame deposition. Notably, the

flame temperature is ca. 1000 °C at HAB of 6 cm and the longer deposition time will eventually damage the FTO decreasing its conductivity.

The performance of $WO_3$ film synthesized at different HAB is also investigated. The curves of current density vs. potential (J-V) for 15 s of $WO_3$ film at HAB of 8 cm and 20 s of $WO_3$ film at HAB of 10 cm are plotted in Figure 3b. Due to the weak mechanical stability on FTO substrate, the 20 s of $WO_3$ deposited at a HAB of 10 cm displays poor performance with very weak current density even after post-calcination treatment (Figure S3b). It was found that $WO_3$ film peeled off from FTO substrate after potential scan. The limited mechanical stability is not improved even after the post-calcination treatment, which impedes its further PEC investigation. When the deposition HAB was reduced to 8 cm, the current density reached 0.75 mA $cm^{-2}$ at 1.24 V vs. RHE. This was much higher than the same $WO_3$ film without post-calcination treatment (0.36 mA $cm^{-2}$ at 1.24 V, Figure S3b), suggesting that the calcination treatment can reduce the defect density, further increase the crystal size from 13.1 to 19.6 and 19.4 to 34.7 nm for the films deposited at HABs of 10 and 8 cm, respectively (Figure S4), and interparticle contacts and/or improve the contact between the interface of $WO_3$ and the FTO substrate, which further facilitate the excited charge transfer.[2e] Because the deposition rate is higher at low HAB,[12] here, different aerosol deposition times were chosen in order to guarantee that the thicknesses of $WO_3$ films at different HAB are comparable with each other. From the comparison, it can be observed that the as-prepared 10s of $WO_3$ films deposited at an HAB of 6 cm demonstrate significant higher current density than that of the $WO_3$ films at HAB of 8 and 10 cm even after post-calcination. This is tentatively attributed to the better grain-boundary interconnectivity of the HAB of 6 cm films, which may improve the photo-excited charges transfer efficiency across the film structure. A control experiment was carried out to investigate the impact of the calcination treatment on the current density of the $WO_3$ films deposited at a HAB of 6 cm. As shown in Figure S3a, there is a slight decrease of the current density after the calcination treatment, indicating that the 10s $WO_3$ film deposited at a HAB of 6 cm has already been sufficiently sintered during the deposition.[13] On the other side, the impact of the necking treatment, previously widely investigated for -$Ta_3N_5$, has been further explored, here, for the $WO_3$ film deposited at a HAB of 8 cm. As shown in Figure S5, the current density increases significantly from 0.75 to 0.9 mA $cm^{-2}$ at 1.23 V vs. RHE after

the necking treatment is applied to the 15s of $WO_3$ films deposited at a HAB of 8 cm. This is comparable to that of $WO_3$ film at HAB of 6 cm and further confirms the importance of the grain boundary interconnectivity for the efficient separation and collection of the photo-generated electrons/holes. Decreasing the HAB below 6 cm broke the FTO and thus was not investigated. Two other different fabrication methods were also adopted for the fabrication of $WO_3$ films to provide a comparison with the flame-deposited films. The morphologies and XRD patterns of the $WO_3$ films fabricated by drop-casting and sputtering are presented in Figure S6 and S7. As shown in Figure 3b, $WO_3$ film fabricated by drop-casting had higher photocurrent density than the $WO_3$ films fabricated by sputtering, but still much lower than that of the 10s flame-made $WO_3$ films deposited at HAB of 6 cm. Considering the very short deposition time of only 10 s and the no-need for other calcination treatments, this flame synthesis method is a one-step ultra-rapid approach that can be easily scaled up for the production of $WO_3$ films with high PEC performance.

The stability of 10s of $WO_3$ film at HAB of 6 cm was investigated by monitoring the current density vs. time. As shown in Figure 3c, the current density of $WO_3$ film at HAB of 6 decreases from initial 0.77 to 0.62 mA $cm^{-2}$ after 1 h of measurement at 1.24 V. In contrast, $WO_3$ films at HAB of 8 cm decreased by 56.5% from initial 0.64 to 0.36 mA $cm^{-2}$ within 1 hours of measurement, which indicates that the $WO_3$ film obtained at HAB of 6 cm has improved stability.

In order to analyze the underlying reasons of the higher performance of the $WO_3$ films obtained at HAB of 6 cm, the electrochemical active surface areas of all the $WO_3$ photoanodes were firstly measured via cyclic voltammograms with various scan rates (Figure S8a). After fitting the linear curve for the capacitive currents at different scan rates, the slope values can be computed with the larger slope value indicating larger electrochemical active surface area.[10] After normalization of the slope values, it can be clearly seen that 15s of $WO_3$ film at HAB of 8 cm has the largest electrochemical active surface areas amongst all the $WO_3$ films fabricated by flame or by the other two methods. However, the current density of the films obtained at HAB of 8 cm is lower than that obtained at 6 cm HAB (Figure S8b). This indicates that the electrochemical active surface area is not the main contributor to the higher current density of the best performing $WO_3$ films (10 s at HAB of 6 cm).

To further explore the main factors contributing to the PEC performance of these photoanodes, the porosities of various $WO_3$ films were calculated (Figure S9). The porosity of flame-made $WO_3$ film could be tuned from ca. 59% to 77% by varying the deposition HAB. The relationship between the porosity and current density is shown in Figure 3d. It can be seen that the current density gradually increased with the porosity increasing from 28% to 59% and decreased with the porosity increasing from 67.8% to 77.5%. This suggests that nor porosity or surface area are the key contributors to the performance of the 10s $WO_3$ films at HAB of 6 cm, which have the highest current density. This is also in line with the analysis of aforementioned electrochemical active surface areas (Figure S8b). Mott-Schottky (MS) and electrochemical impedance spectroscopy (EIS) measurements were also conducted with the flame-made $WO_3$ films fabricated at different HAB. The MS curves of the $WO_3$ films deposited for 10 s and 15 s at HAB of 6 and 8 cm, respectively, are shown in Figure 4a. Both samples show positive slopes in the MS plots indicating a n-type semiconductor behaviour.[2a] Meanwhile, the $WO_3$ film at HAB of 6 cm show substantially smaller slope compared to that of $WO_3$ film at HAB of 8 cm, indicating significantly increased donor densities.[5e] Based on the MS equation, the donor densities of the $WO_3$ film at HAB of 6 cm is calculated to be $9.44 \times 10^{20}$ $cm^{-3}$, around 1.7 time higher than that of the $WO_3$ film at HAB of 8 cm. From the comparison, it is suggested that $WO_3$ film fabricated at HAB of 6 cm might have higher oxygen vacancies than that of post-calcinated $WO_3$ film fabricated at HAB of 8 cm, and thus benefit of improved charge transport in $WO_3$ and at the interface between FTO and $WO_3$.[2a, 5e] In order to prove the oxygen vacancies, Raman analysis of the flame-made films was performed for the different HABs (Figure S10). Two strong Raman peaks located at 804 and 715 $cm^{-1}$ are assigned to the $\nu(O–W^{6+}–O)$ vibrational stretching mode of the W-O-W bridging oxygen and a medium strong peak at ~ 272 $cm^{-1}$ is associated with $\delta(O–W^{6+}–O)$ bending mode, while the weak peaks at ~ 326 $cm^{-1}$ and ~ 449 $cm^{-1}$ correspond to the vibrations of the $O–W^{5+}–O$ and $W^{5+}=O$ bonds,[14] respectively, indicating the presence of oxygen vacancies.[15] Notably, the $WO_3$ film deposited at a HAB of 6 cm shows the highest Raman spectra intensity ratio for the two peaks related to the oxygen vacancies related, indicating that the $WO_3$ film at HAB of 6 cm has higher oxygen vacancies than those obtained at the other HABs. It is also possible that

the preferential [020] direction of the $WO_3$ at HAB of 6 cm increases the electron mobility and hence, the electron transport properties.[10]

The EIS measurements were conducted to evaluate the kinetics of charge transfer for the $WO_3$ films. The Nyquist diagrams in the frequency range of 100 kHz-10 mHz for $WO_3$ films at HAB of 6 cm and $WO_3$ films at HAB of 8 cm are shown in Figure 4b. The equivalent circuit of Randle circuit is also displayed in the inset, in which $R_s$ is the solution resistance, $R_{ct}$ is the charge transfer resistance across the interface of electrode/electrolyte, and CPE is the constant phase element for the electrolyte/electrode interface.[16] The arcs in the Nyquist plot are related to charge transfer at interface of $WO_3$/electrolyte. The fitted values of $R_{ct}$ were 899 and 958.7 Ω for $WO_3$ films at HAB of 6 cm and $WO_3$ films at HAB of 8 cm, respectively. The $WO_3$ films at HAB of 6 cm has a high charge transfer efficiency showing a lower $R_{ct}$ value than that of $WO_3$ films at HAB of 8 cm. Efficient charge transfer at the $WO_3$/electrolyte interface can also hinder charges recombination.[16]

To evaluate the impact of the flame exposure on the conductivity of FTO substrates, a series of EIS measurements were also carried out and the $R_s$ values were compared. $R_s$ is deduced as solution resistance, but it can also be used to indirectly evaluate the conductivity of FTO substrates if the experimental condition keeps the same except of the working electrodes. As shown in Figure below, $R_s$ are analysed as 23.8, 26.8, 33.8, 36.5 ohms for the bare FTO, FTO exposed to a nanoparticle-free flame at a HAB of 10 cm, at a HAB of 8 cm, and at a HAB of 6 cm, respectively. This indicates that exposure of the substrate to the flame increases the resistance of FTO substrates. However, as the deposition time is very short, the resistance of the FTO even at low HAB is still sufficiently low. In order to further investigate whether the deposition of the $WO_3$ films influenced the resistance of FTO substrates, the $R_s$ values are also deduced after the deposition of $WO_3$ films at different HAB. It was found that the $R_s$ values are 23.9 and 25.8 ohms for the $WO_3$ films deposited at a HAB of 8 and 6 cm, respectively, which are comparable to that of the bare FTO substrates. This suggests that the deposition of $WO_3$ films can act as a protective layer inhibiting the direct flame contact to the FTO substrate and its damage. Overall, there is no obvious impact on the conductivity of FTO substrates for the deposition of $WO_3$ films at different HAB within the deposition time utilized here.

The incident photon-to-current conversion efficiency (IPCE) spectrum of the $WO_3$ film made at a HAB of 6 and 8 cm were further investigated. As shown in Figure 4c, the $WO_3$ film at HAB of 6 cm shows a rising IPCE from 460 nm, in line with its bandgap, and reaches a maximum IPCE of ca. 61% at 360 nm This is significantly higher than that obtained with $WO_3$ films deposited at a HAB of 8 cm (~ 45% at 360 nm).

The PEC performance of the $WO_3$ films deposited at a HAB of 6 cm was compared to state-of-the-art $WO_3$ photoanodes in Table 1. The current density of the flame-made $WO_3$ photoanodes can reach 0.91 mA $cm^{-2}$ at 1.24 V vs. RHE, which is comparable to some of the best pure $WO_3$ photoanodes reported.[2c, 5e-h, 10, 17] Notably, most of the synthesis methods require several hours for fabrication and also needs a post-calcination treatment to further increase the film crystallinity.[2c, 5e-h, 10, 17] In contrast, the flame deposition method presented here requires 10 s for the fabrication of efficient $WO_3$ photoanodes without the need of any post-calcination treatments. The superior PEC performance of the $WO_3$ deposited at a HAB of 6 cm is closely connected with its high deposition temperature (~1000 $^{o}$C). This results in both a robust film morphology and more oxygen vacancies which improve the charge-transfer efficiency across the $WO_3$/electrolyte interface, and results in higher current density and high IPCE. Furthermore, the ultra-rapid fabrication process (10 s) at HAB of 6 cm enables to avoid damage to the FTO substrate. In contrast, the $WO_3$ films fabricated at HAB of 8 and 10 cm are more porous and thus have higher surface areas than that at HAB of 6 cm. However, the low donor densities, and high charge recombination at the interface and the poorer mechanical stability greatly diminish their PEC performance. Notably, flame synthesis is a flexible method that can be easily scaled up and extended to fabricate other metal oxide based photoelectrodes without any post-calcination treatment.

## CONCLUSION

We have reported a one-step ultra-rapid flame-based method for the fabrication of efficient $WO_3$ photoanodes for water oxidation. A short deposition time of 10 s is sufficient for the fabrication of robust $WO_3$ films that do not require post-calcination treatment and achieve a photocurrent density for water oxidation of 0.91 $mAcm^{-2}$ at 1.24 V vs RHE in 0.1M $H_2SO_4$ and an IPCE of ~ 61% at 360 nm. Optimization of the structural properties of these flame-made $WO_3$ films reveal that the high deposition

temperature achieved for short time at a height above the nozzle of 6 cm improves the film donor concentration and charge-transfer efficiency without damaging the FTO substrates. This results in a significantly better performance than that of flame-made films deposited at higher height above the burner or fabricated by other methods such as sputtering or drop-casting of the same flame-made $WO_3$ particles. These findings provide a flexible and scalable one-step approach for the rapid fabrication of robust photoanodes made of earth-abundant low cost metal oxides such as $WO_3$ and $Fe_3O_2$.

## METHODS

**Synthesis of $WO_3$ photoelectrodes**. A flame spray pyrolysis (FSP) system was used for the direct deposition of $WO_3$ film onto FTO substrates or collection of $WO_3$ powder on a filter paper for the fabrication of drop-casting photoelectrode. The detailed procedures were prepared as follows: The FTO glass (PV-TECH, 7 $\Omega$ $cm^{-1}$) was cleaned with soap water, acetone and 2-propanol sequentially. A total W-metal atom concentration of 0.2 mol $L^{-1}$ was prepared by dissolving ammonium (meta) tungstate hydrate (Aldrich, purity > 97%) in a 1:1 (volume ratio) mixture of diethylene glycol monobutyl ether (Aldrich, purity > 98.5%) and ethanol (Aldrich, purity > 99.5%). This solution was supplied through a syringe pump at a rate of 5 mL $min^{-1}$, and dispersed into a fine spray with 7 L $min^{-1}$ oxygen at a constant pressure drop of 2 bars. The spray was ignited by supporting premixed methane/oxygen flames ($CH_4$ = 1.2 L $min^{-1}$, $O_2$ = 2 L $min^{-1}$). A substrate holder placed at different height above the burner (HAB) was utilized for the deposition of $WO_3$ films on FTO substrates with different controlled time. With the exception of the $WO_3$ deposited at an HAB of 6 cm, the rest $WO_3$ photoelectrodes were sintered at 500 $^oC$ for 2 h with 5$^oC$ ramming rate under air environment. The drop-casting $WO_3$ film was fabricated by dispersing 50 mg of $WO_3$ powder in 1 mL of ethanol, then take 100 µL of mixed solution and drop-cast on FTO substrates until it is totally dry for further post-calcination treatment.

$WO_3$ was deposited on FTO films by a DC magnetron sputtering system (AJA ATC 2400) using 99.99% pure W metal as a target, Ar as a sputtering gas, and $O_2$ as a reactive gas with the gas flow Ar/$O_2$ 18/2 sccm. The chamber was evacuated to a base pressure of $9 \times 10^{-7}$ Torr before deposition. Sputtering deposition was performed at a gas pressure of $4 \times 10^{-3}$ Torr for 120 minutes at room temperature with a power of 200 W. The as-prepared films were annealed in a furnace at 500 °C for 2 h at ambient pressure prior to run PEC test.

**PEC measurement and Characterizations**. The PEC measurements were performed in a home-made one-compartment reactor with a quartz window. A three-electrode configuration was used with Pt wire, Ag/AgCl electrode, and FTO/$WO_3$ as the counter, reference, and working electrodes, respectively. A 0.1 M of $H_2SO_4$ solution (pH = 0.69) was used as the electrolyte and all the potential values have been reported vs. RHE based on $V_{RHE} = V_{Ag/AgCl} + 0.059pH + E_{Ag/AgCl}$. Amperometric J-T curves were measured at 1 V vs. Ag/AgCl on an Electrochemical Workstation (CHI 660E, USA). A xenon lamp (NewSpec, LCS-100) with an AM 1.5G filter was used as the light source for the measuring the photocurrent. The illumination area was set by an aperture to 0.785 $cm^2$. The Mott–Schottky analysis was performed in a three-electrode configuration in 0.1 M of $H_2SO_4$ solution with 1 kHz frequency in the dark. EIS was conducted using a 5 mV amplitude perturbation of between 100K and 0.01 Hz with an applied voltage of 0.4 V vs. Ag/AgCl under light illumination in a three-electrode configuration.

The morphology and EDS was investigated by using Zeiss Ultraplus (FESEM) at 3 kV. The crystallinity was characterized by X-ray diffraction using Bruker system (XRD, D 2 Phaser, USA) equipped with Cu Kα radiation of average wavelength 1.54059 Å. The absorbance spectra were measured with a Perkin–Elmer (Lambda 1050 UV/vis/NIR) Spectrophotometer and a 150 mm integrating sphere. Raman spectra of $WO_3$ films were collected using IM-52 Raman microscope (Snowy Range) with 785 nm laser excitation under 40X objective. The laser power of 70 mW and integration time of 0.5 second were applied for all the samples. The capacitive current was measured by using cyclic voltammograms within potential range between 0.4 to 0.6 V vs. Ag/AgCl with various scan rates in a 0.1 M $H_2SO_4$. The porosities of $WO_3$ films were calculated based on their average mass divided by the bulk mass of $WO_3$ (density, 7.16 g/cm³) with the same of volume.

## AUTHOR INFORMATION


### Corresponding Authors

*Email: antonio.tricoli@anu.edu.au;

*Email:hongjun.chen@anu.edu.au;


### Author Contributions

R.B., T.T. and H.C. performed materials synthesis, characterization and PEC measurements. H.C., G.L and A.T. contributed to the writing of the manuscript. All authors contributed to the data analysis.

### Notes

The authors declare no competing financial interest.

## ACKNOWLEDGEMENTS

A.T. gratefully acknowledges the support of Australian Research Council (ARC) DP150101939, ARC DE160100569, and Westpac 2016 Research Fellowship, H.C. and A.T. thanks N.N. for the EDS measurement.

## REFERENCES


[1] M. G. Walter, E. L. Warren, J. R. McKone, S. W. Boettcher, Q. Mi, E. A. Santori, N. S. Lewis, *Chem. Rev.* **2010**, *110*, 6446-6473.

[2] a) H. Chen, G. Liu, L. Wang, *Sci. Rep.* **2015**, *5*, 10852; b) P. Peerakiatkhajohn, J.-H. Yun, H. Chen, M. Lyu, T. Butburee, L. Wang, *Adv. Mater.* **2016**, *28*, 6405-6410; c) S. Wang, H. Chen, G. Gao, T. Butburee, M. Lyu, S. Thaweesak, J.-H. Yun, A. Du, G. Liu, L. Wang, *Nano Energy* **2016**, *24*, 94-102; d) G. Wang, X. Yang, F. Qian, J. Z. Zhang, Y. Li, *Nano Lett.* **2010**, *10*, 1088-1092; e) H. Chen, M. Lyu, M. Zhang, K. Feron, D. J. Searles, M. Dargusch, X. Yao, L. Wang, *ChemSusChem* **2017**, *10*, 670-674.

[3] a) Q. Mi, A. Zhanaidarova, B. S. Brunschwig, H. B. Gray, N. S. Lewis, *Energy Environ. Sci.* **2012**, *5*, 5694-5700; b) T. Zhu, M. N. Chong, E. S. Chan, *ChemSusChem* **2014**, *7*, 2974-2997.

[4] C. Liu, N. P. Dasgupta, P. Yang, *Chem. Mater.* **2014**, *26*, 415-422.

[5] a) C. Santato, M. Odziemkowski, M. Ulmann, J. Augustynski, *J. Am. Chem. Soc.* **2001**, *123*, 10639-10649; b) S. H. Baeck, K. S. Choi, T. F. Jaramillo, G. D. Stucky, E. W. McFarland, *Adv. Mater.* **2003**, *15*, 1269-1273; c) S. Berger, H. Tsuchiya, A. Ghicov, P. Schmuki, *Appl. Phys. Lett.* **2006**, *88*, 203119; d) E. L. Miller, B. Marsen, D. Paluselli, R. Rocheleau, *Electrochem. Solid State Lett.* **2005**, *8*, A247-A249; e) G. Wang, Y. Ling, H. Wang, X. Yang, C. Wang, J. Z. Zhang, Y. Li, *Energy Environ. Sci.* **2012**, *5*, 6180-6187; f) J. Su, X. Feng, J. D. Sloppy, L. Guo, C. A. Grimes, *Nano Lett.* **2011**, *11*, 203-208; g) P. M. Rao, L. Cai, C. Liu, I. S. Cho, C. H. Lee, J. M. Weisse, P. Yang, X. Zheng, *Nano Lett.* **2014**, *14*, 1099-1105; h) Y. Hou, F. Zuo, A. P. Dagg, J. Liu, P. Feng, *Adv. Mater.* **2014**, *26*, 5043-5049; i) J. Su, L. Guo, N. Bao, C. A. Grimes, *Nano Lett.* **2011**, *11*, 1928-1933.

[6] a) R. Strobel, S. E. Pratsinis, *J. Mater. Chem.* **2007**, *17*, 4743-4756; b) R. Strobel, S. E. Pratsinis, *Nanoscale* **2007**, *17*, 4743-4756.

[7] A. Tricoli, M. Righettoni, A. Teleki, *Angew. Chem. Int. Ed.* **2010**, *49*, 7632-7659.

[8] a) N. Nasiri, R. Bo, F. Wang, L. Fu, A. Tricoli, *Adv. Mater.* **2015**, *27*, 4336-4343; b) A. Tricoli, M. Graf, F. Mayer, S. Kuühne, A. Hierlemann, S. E. Pratsinis, *Adv. Mater.* **2008**, *20*, 3005-3010.

[9] A. Tricoli, N. Nasiri, H. Chen, A. S. Wallerand, M. Righettoni, *Solar Energy* **2016**, *136*, 553-559.

[10] S. Shin, H. S. Han, J. S. Kim, I. J. Park, M. H. Lee, K. S. Hong, I. S. Cho, *J. Mater. Chem. A* **2015**, *3*, 12920-12926.

[11] C. Ng, Y. H. Ng, A. Iwase, R. Amal, *ACS Appl. Mater. Interfaces* **2013**, *5*, 5269-5275.

[12] R. Bo, N. Nasiri, H. Chen, D. Caputo, L. Fu, A. Tricoli, *ACS Appl. Mater. Interfaces* **2017**, *9*, 2606-2615.

[13] M. Higashi, K. Domen, R. Abe, *Energy Environ. Sci.* **2011**, *4*, 4138-4147.

[14] S.-H. Lee, H. M. Cheong, P. Liu, D. Smith, C. E. Tracy, A. Mascanrenhas, J. R. Pitts, S. K. Deb, *J. Appl. Phys.* **2000**, *88*, 3076-3078.

[15] E. Valova, J. Georgieva, S. Armyanov, S. Sotiropoulos, A. Hubin, K. Baert, M. Raes, *J. Electrochem. Soc.* **2010**, *157*, D309-D315.

[16] S. J. Hong, S. Lee, J. S. Jang, J. S. Lee, *Energy Environ. Sci.* **2011**, *4*, 1781-1787.

[17] a) Y. Pihosh, I. Turkevych, K. Mawatari, T. Asai, T. Hisatomi, J. Uemura, M. Tosa, K. Shimamura, J. Kubota, K. Domen, T. Kitamori, *Small* **2014**, *10*, 3692-3699; b) W. Li, P. Da, Y. Zhang, Y. Wang, X. Lin, X. Gong, G. Zheng, *ACS Nano* **2014**, *8*, 11770-11777; c) T. Zhang, Z. Zhu, H. Chen, Y. Bai, S. Xiao, X. Zheng, Q. Xue, S. Yang, *Nanoscale* **2015**, *7*, 2933-2940; d) Y. Liu, J. Li, W. Li, Y. Yang, Y. Li, Q. Chen, *J. Phys. Chem. C* **2015**, *119*, 14834-14842; e) J. Zhang, P. Zhang, T. Wang, J. Gong, *Nano Energy* **2015**, *11*, 189-195; f) Y. Liu, L. Zhao, J. Su, M. Li, L. Guo, *ACS Appl. Mater. Interfaces* **2015**, *7*, 3532-3538; g) X. Feng, Y. Chen, Z. Qin, M. Wang, L. Guo, *ACS Appl. Mater. Interfaces* **2016**, *8*, 18089-18096.

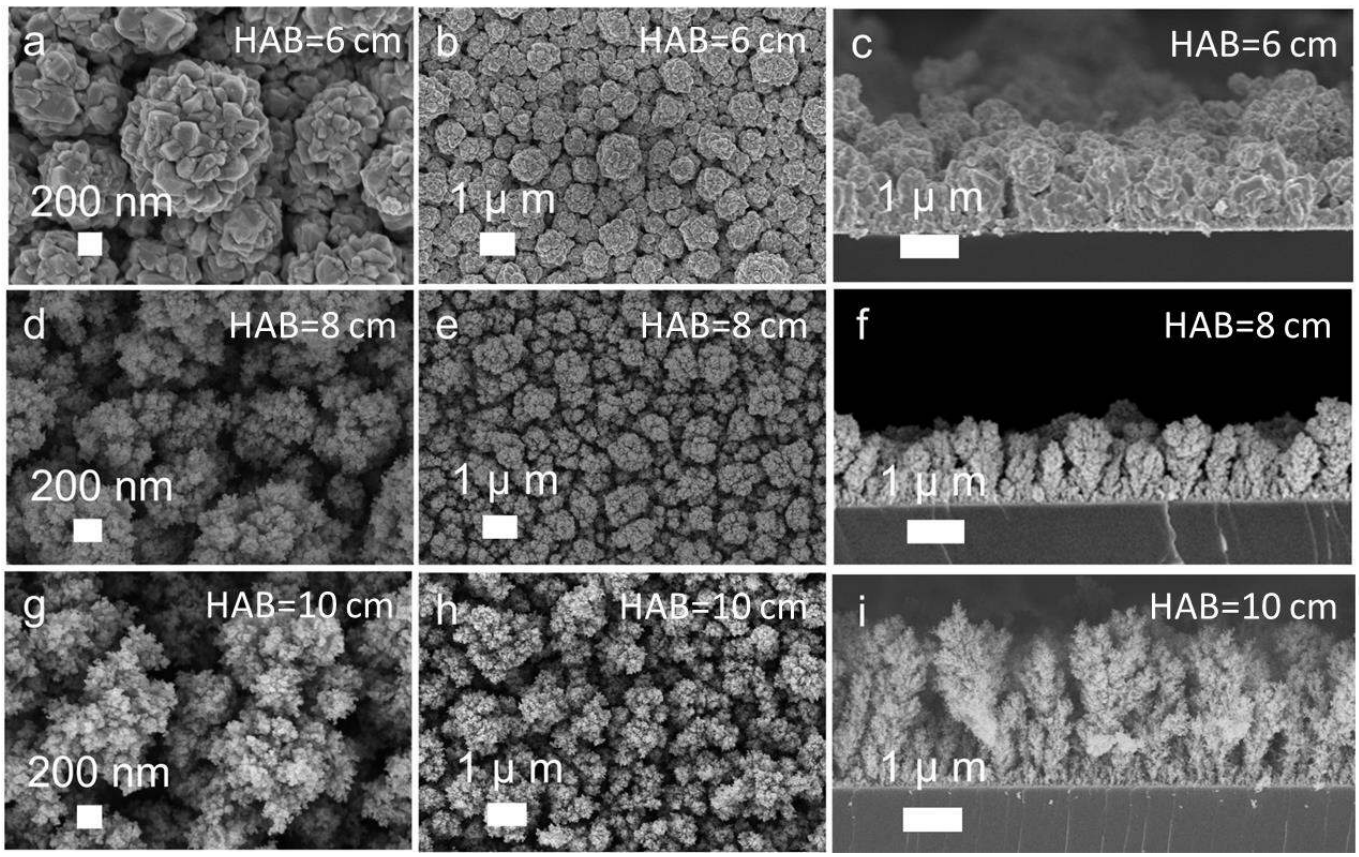


**Figure 1. Morphological characterization of $WO_3$ films.** typical top-view SEM images of $WO_3$ films deposited at HAB of 6 cm (a-b), 8 cm (d-e) and 10 cm (g-h) with different magnifications and their corresponding cross-sectional SEM images (c, f, i).

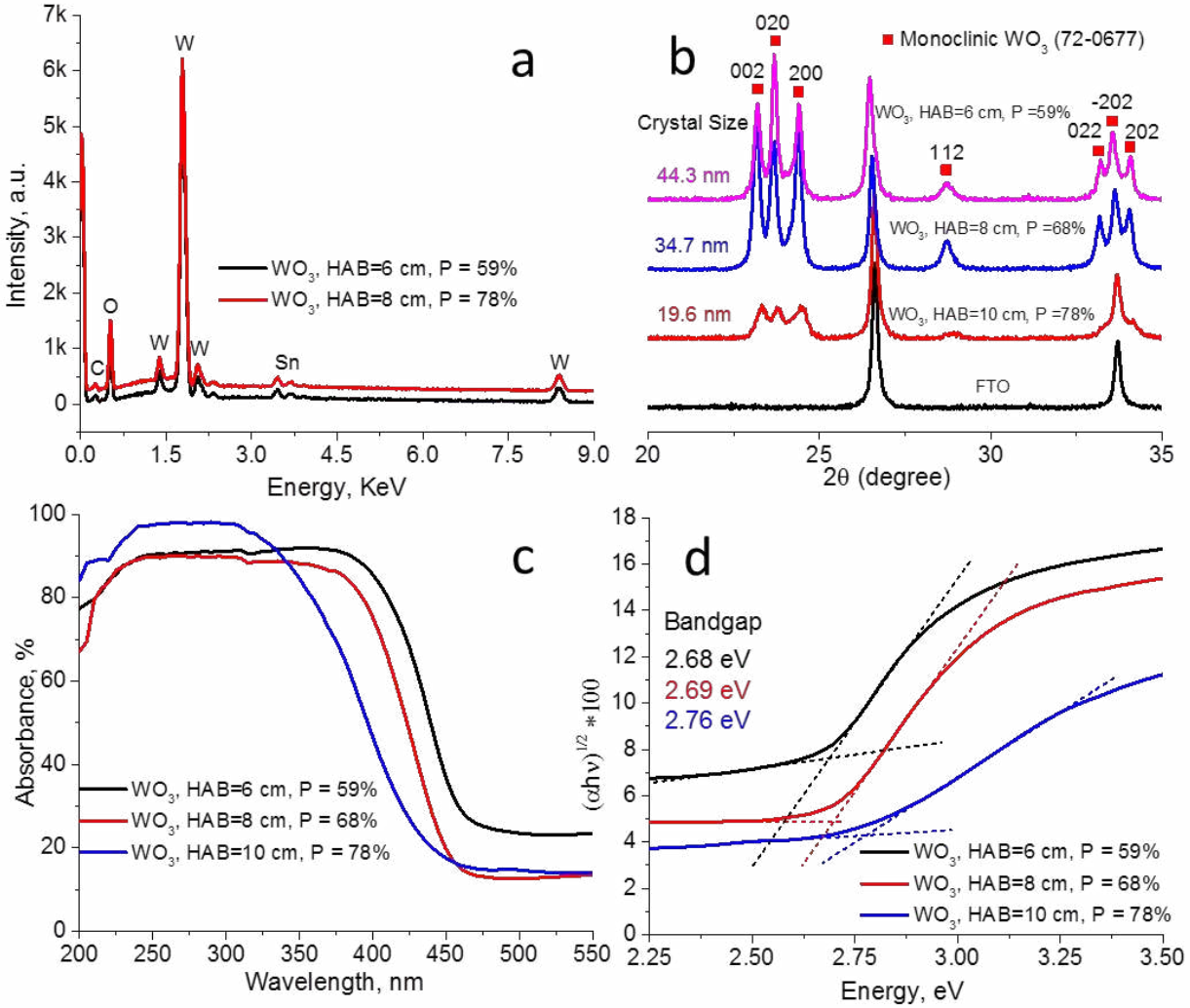


**Figure 2. Structural and optical characterizations of $WO_3$ films.** a, EDS, b, XRD, c, UV-vis spectra, d, Trauc plots of various $WO_3$ films deposited at different HAB and their corresponding porosity (P).

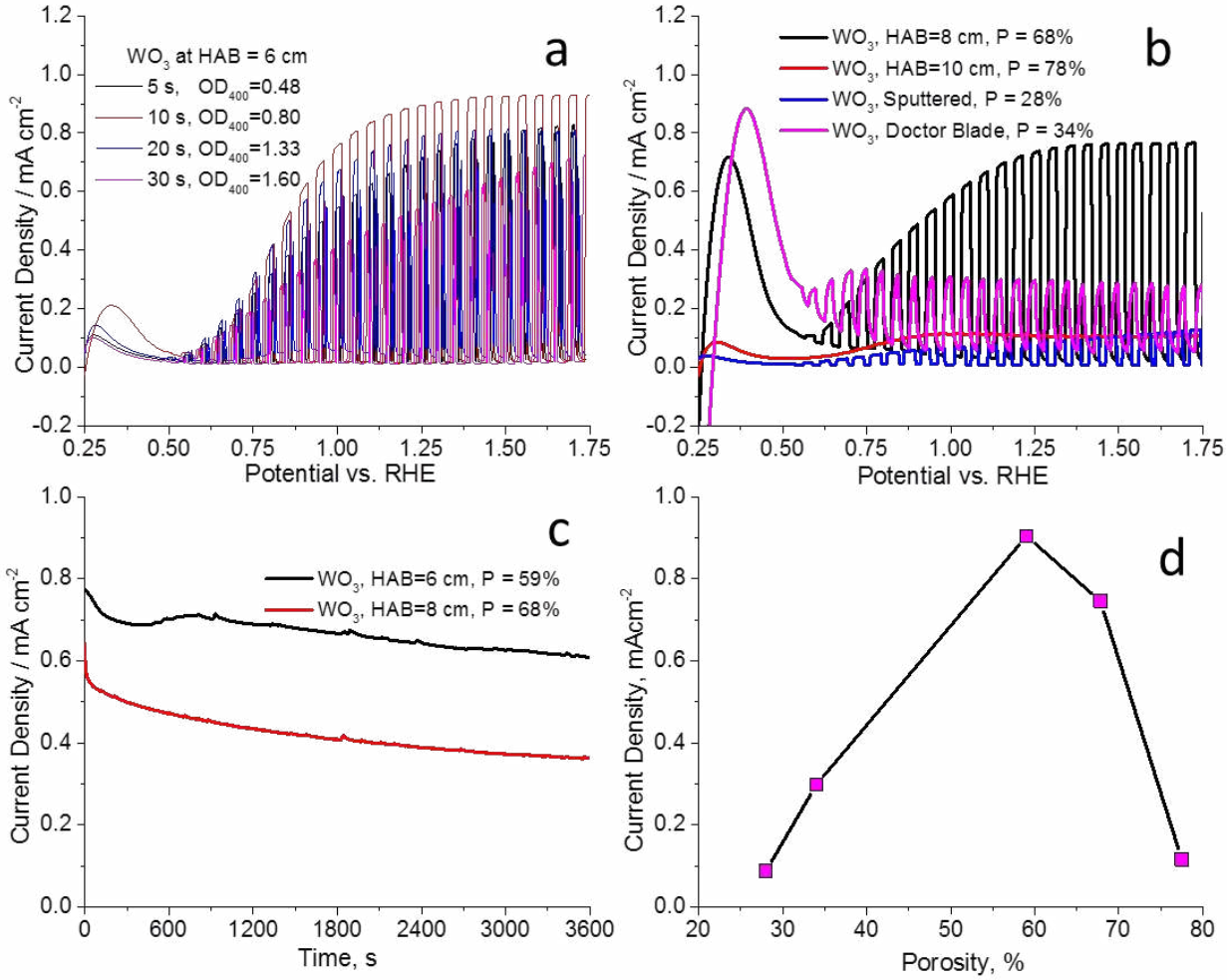


**Figure 3. PEC performance of the $WO_3$ films.** (a) J-V curves of $WO_3$ film fabricated at HAB of 6 cm with different deposition time; (b) J-V curves of $WO_3$ film fabricated at different HAB and different methods; (c) Chronoamperometry of $WO_3$ films at HAB of 6 cm and 8 cm at an applied potential of 1.24 V vs. RHE; (d) the relationship between the current density of $WO_3$ films fabricated by different methods with their porosities (d).

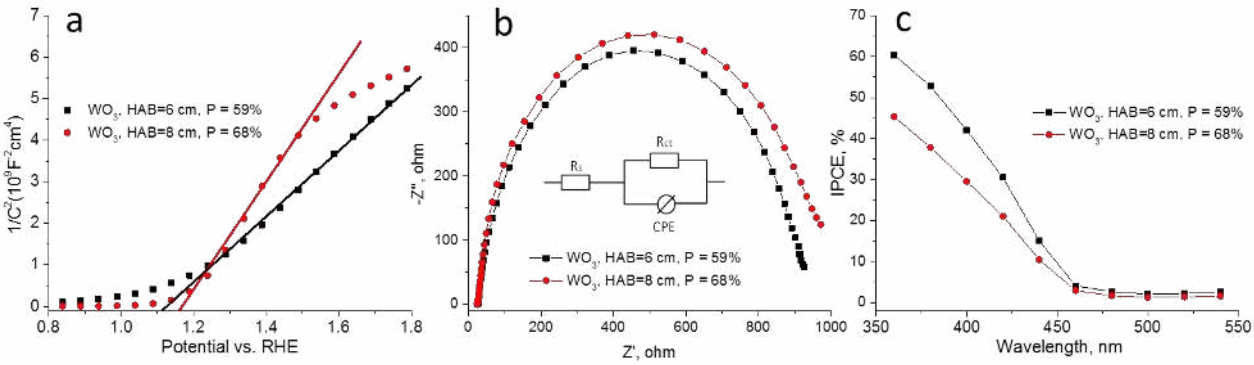


**Figure 4. Electrochemical characterizations of $WO_3$ films.** (a) Mott–Schottky plots measured at 1 kHz in the dark; (b) Nyquist plots collected at 0.64 V vs. RHE under illumination; The inset provides the equivalent circuit used to fit the impedance data. (c) Wavelength dependence of IPCE measurement at 1.24 V vs. RHE.

**Table 1.** Comparison of the state-of-art $WO_3$ photoanode for PEC water splitting.

| Material | Method/total fabrication time including post-treatment | Electrolyte (Light source) | Current density | Reference |
|---|---|---|---|---|
| $WO_3$ film | Flame Nanoparticle Aerosol Deposition/10 s | 0.1M $H_2SO_4$ (AM 1.5 G) | 0.91 mA $cm^{-2}$ at 1.23V vs. RHE | This work |
| $WO_3$ nanoflake arrays | Hydrothermal / > 6 h | 0.1 M $Na_2SO_4$ AM 1.5 G | 1.43 mA $cm^{-2}$ vs ~1.2 V vs. Pt | 5f |
| Hydrogen-treated $WO_3$ nanoflakes | Hydrothermal / > 7 h | 0.5 M $Na_2SO_4$ AM 1.5 G | 0.88 mA $cm^{-2}$ at 1.6 V vs. RHE | 5e |
| $WO_3$ nanosheet array | Hydrothermal / > 6 h | 0.01M $Na_2SO_4$ AM 1.5 G | ~0.68 mA $cm^{-2}$ at 1.23 V vs. RHE | 5h |
| $WO_3$ NWs | Flame vapor deposition / > 2.5 h | 0.5 M potassium phosphate (pH = 8) AM 1.5 G | 1.1 mA $cm^{-2}$ at 1.23 V vs. RHE | 5g |
| $WO_3$ nanorods | Glancing angle deposition / > 7 h | 0.5 M $Na_2SO_4$ (pH = 7), AM 1.5 G | 0.55 mA $cm^{-2}$ at 1.23 V vs. RHE | 17a |
| Dual etched/reduced $WO_3$ Nanoflakes | Hydrothermal / > 8 h | 1M $H_2SO_4$ AM 1.5 G | ~1.10 mA $cm^{-2}$ at 1.23 V vs. RHE | 17b |
| Pristine $WO_3$ | Hydrothermal / > 4 h | | ~0.62 mA $cm^{-2}$ at 1.23 V vs. RHE | |
| Fe-doped $WO_3$ nanoflakes | Hydrothermal / > 7 h | 0.1 M $Na_2SO_4$ AM 1.5 G | 0.88 mA $cm^{-2}$ at 1.23 V vs. RHE | 17c |
| Pristine $WO_3$ nanoflakes | Hydrothermal / > 7 h | | 0.69 mA $cm^{-2}$ at 1.23 V vs. RHE | |
| Gd-doped−$WO_3$ vertical arrays | Hydrothermal / > 13 h | 0.2 M $Na_2SO_4$ AM 1.5 G | 2.28 mA $cm^{-2}$ at 1.6 V vs. RHE | 17d |
| pristine $WO_3$ vertical arrays | | | 0.90 mA $cm^{-2}$ at 1.6 V vs. RHE | |
| $WO_3$ nanomultilayers | Hydrothermal / > 8 h | 0.5 M $Na_2SO_4$ AM 1.5 G | ~ 0.88 mA $cm^{-2}$ at 1.23 V vs. RHE | 17e |
| Porous $WO_3$ nanorod array | Hydrothermal / > 8 h | 0.5 M $Na_2SO_4$ AM 1.5 G | ~ 0.6 mA $cm^{-2}$ at 1.23 V vs. RHE | 17f |
| Tree-like nanoporous $WO_3$ | Pulsed laser deposition / >2.5 h | 0.5 M phosphate buffer solution (pH 7.0) | 1.8 mA $cm^{-2}$ at 1.23V vs. RHE | 10 |

| | | | | |
|---|---|---|---|---|
| $WO_3$ plate-like array | Hydrothermal / > 18 h | 0.1M $H_2SO_4$ AM 1.5 G | 3.7 $mAcm^{-2}$ at 1.23V vs. RHE | 2c |
| $WO_3$ nanoplate arrays | Hydrothermal / > 6 h | 0.5 M $Na_2SO_4$ AM 1.5 G | ~ 1 mA $cm^{-2}$ at 1.23 V vs. RHE | 17g |

**Entry for the Table of Contents** (Please choose one layout)

## COMMUNICATION

One-step ultra-rapid scalable method for the fabrication of efficient $WO_3$ photoanodes were fabricated through flame-made nanoparticle aerosols. A short deposition time of 10 s was sufficient for the fabrication of robust $WO_3$ films that do not require post-calcination treatment and achieve a photocurrent density for water oxidation of 0.91 $mAcm^{-2}$ at 1.24 V vs RHE in 0.1M $H_2SO_4$, and an IPCE of ~ 61% at 360 nm.

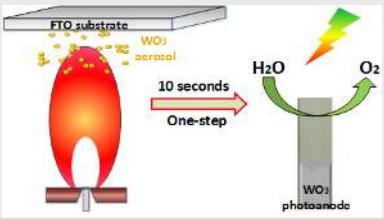


*Hongjun Chen*, Renheng Bo, Thanh Tran-Phu, Guanyu Liu and Antonio Tricolia**

***Page No. – Page No.***

**One-step Rapid and Scalable Flame Synthesis of Efficient $WO_3$ Photoanodes for Water Splitting**